Science
AAAS

Air-Stable All-Inorganic Nanocrystal Solar Cells Processed from Solution

Ilan Gur, *et al.*

Science **310**, 462 (2005);
DOI: 10.1126/science.1117908

CORRECTED 9 DECEMBER 2005; SEE LAST PAGE

Air-Stable All-Inorganic Nanocrystal Solar Cells Processed from Solution

Ilan Gur,[1,3] Neil A. Fromer,[1] Michael L. Geier,[3] A. Paul Alivisatos[1,2]*

We introduce an ultrathin donor-acceptor solar cell composed entirely of inorganic nanocrystals spin-cast from solution. These devices are stable in air, and post-fabrication processing allows for power conversion efficiencies approaching 3% in initial tests. This demonstration elucidates a class of photovoltaic devices with potential for stable, low-cost power generation.

Organic materials offer strong potential for cost reduction vis-à-vis conventional solar cells, but their spectrally limited absorption and low carrier mobilities impose limitations on achieving commercially viable device efficiencies (*1*). Colloidal inorganic nanocrystals share all of the primary advantages of organics—scalable and controlled synthesis, an ability to be processed in solution, and a decreased sensitivity to substitutional doping—while retaining the broadband absorption and superior transport properties of traditional photovoltaic (PV) semiconductors (*2*–*4*). Using inorganic nanocrystals (NCs) for electron transport can enhance the performance of semiconductor polymer solar cells (*5*, *6*), but the ultimate limitations of these hybrid systems may still be dictated by the low mobility and environmental sensitivity of their organic phase. A solar cell that relies exclusively on colloidal NCs has been anticipated theoretically in recent years (*7*, *8*). We now demonstrate such a device and present a mechanism for its operation in the context of organic donor-acceptor (D-A) and conventional p-n junction solar cells.

A well-accepted model has emerged that describes the operation of organic-based solar cells relative to their conventional inorganic counterparts (*7*, *9*). The organic D-A solar cell relies on a type II heterojunction, which serves to dissociate the strongly bound excitons characteristic of organic systems. Materials design for this type of PV system thus requires proper energy band alignment of active materials to facilitate charge transfer. Examples to date have been limited to systems with at least one active organic component (*5*, *10*–*14*). However, studies of type II semiconductor NC heterostructures show that efficient charge transfer may also occur between two such inorganic components with staggered energy levels (*15*, *16*). In addition, recent research has revealed a growing number of similarities between NC films and organic molecular semiconductors. Like organic systems, NC films exhibit extremely low carrier concentrations and high trap densities (*17*, *18*), as well as confined excitations that may migrate between crystals (*19*). All of these properties are sufficient, and some are requisite, for solar energy conversion based on the D-A model (*7*, *9*).

The PV devices described here use rod-shaped CdSe (Fig. 1A) and CdTe (Fig. 1B) NCs that we synthesized and prepared separately (*20*). A schematic energy diagram (Fig. 1C) illustrates the staggered band alignment of this prototypical D-A pair. In fabricating devices, NCs were spin-cast from a filtered pyridine solution, which created ultrathin, flexible films of densely packed NCs on virtually any substrate. Typical films are homogeneous and pinhole-free over large areas (Fig. 1D).

We fabricated planar D-A heterojunctions by sequentially spin-casting films of CdTe and then CdSe on indium tin oxide (ITO) glass coated with 2 Å alumina. Thermally deposited aluminum was used as a reflective top contact. Brief annealing of the CdTe film for 15 min at 200°C removed residual solvent and allowed for subsequent deposition of the CdSe film. In this way, high-quality bilayer structures were formed with minimal intermixing at the interface (*20*).

The photoaction spectrum of a typical bilayer cell (Fig. 2A) reveals features from both the CdSe and CdTe absorption spectra. Thus, both components contribute to the photocurrent. Current-voltage (I-V) characteristics of this device in the dark and at simulated Air Mass 1.5 Global (AM1.5G) full-sun illumination are presented in Fig. 2B. The device exhibits strong photoresponse and diode rectification in the dark and light. In addition, this representative cell exhibits a notable PV effect, with a short-circuit current (I_{sc}) of 0.58 mA/cm^2, open-circuit voltage (V_{oc}) of 0.41 V, and fill factor (*FF*) of 0.40 (*21*).

We can distinguish the solar cells presented here from conventional thin film heterojunction cells. Conventional cells depend on a junction between bulk p- and n- doped materials to form a built-in field, which then acts as the primary driving force for minority carrier extraction (*22*, *23*). Similar to organic semiconductors, colloidal NCs are characterized by extremely limited free-carrier concentrations (*4*). In fact, three-dimensional CdSe colloid arrays have been found to contain essentially no free carriers without illumination (*18*). As such, the creation of a depleted junction in these NC cells is highly unlikely.

In accordance with these prior studies, the CdSe and CdTe films presented here are electrically insulating in the dark. Measuring surface conduction across a 1-mm gap between two aluminum electrodes yields linear IV curves, from which sheet resistances exceeding 500 G-ohms per square, a value

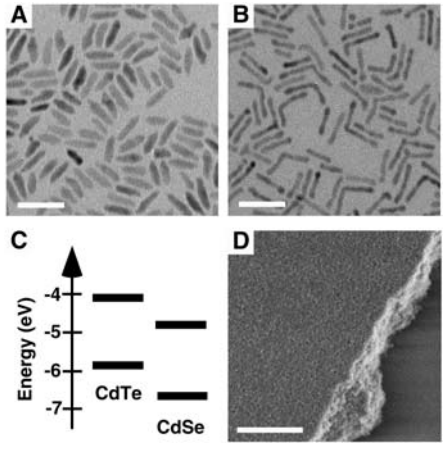

Fig. 1. Transmission electron micrographs of (**A**) CdSe and (**B**) CdTe NCs used in this investigation. Scale bar, 40 nm. (**C**) An energy diagram of valence and conduction band levels for CdTe and CdSe illustrates the type II charge-transfer junction formed between the two materials. Employing the effective mass approximation, bulk energy levels were modified to account for quantum confinement. Valence band edges for CdSe and CdTe rods were calculated to be –4.79 eV and –4.12 eV, respectively. Conduction band edges for CdSe and CdTe rods were calculated to be –6.64 eV and –5.85 eV, respectively. (**D**) A typical spin-cast film of colloidal NCs imaged by scanning electron micrography is homogeneous and defect-free; the film edge of this ~100-nm film is shown for contrast with the silicon substrate. Scale bar, 1 μm.

[1]Materials Science Division, Lawrence Berkeley National Laboratory, Berkeley, CA 94720, USA. [2]Department of Chemistry, [3]Department of Materials Science and Engineering, University of California, Berkeley, CA 94720, USA.

*To whom correspondence should be addressed. E-mail: alivis@berkeley.edu

limited by the measurement apparatus, can be extracted for films of either material on glass substrates. Exposing the films to 100 mW/cm^2 full-sun irradiation effected a marked rise in conductivity. Sheet resistances, now measurable, dropped at least one order of magnitude under illumination. Likewise, illumination afforded a greater than three orders of magnitude enhancement in conductivity of the device itself (Fig. 2B). This strong photoconductive effect suggests that these materials, like their organic counterparts, have an extremely limited number of untrapped carriers in the dark and are better characterized by a rigid band model than by one that employs band bending.

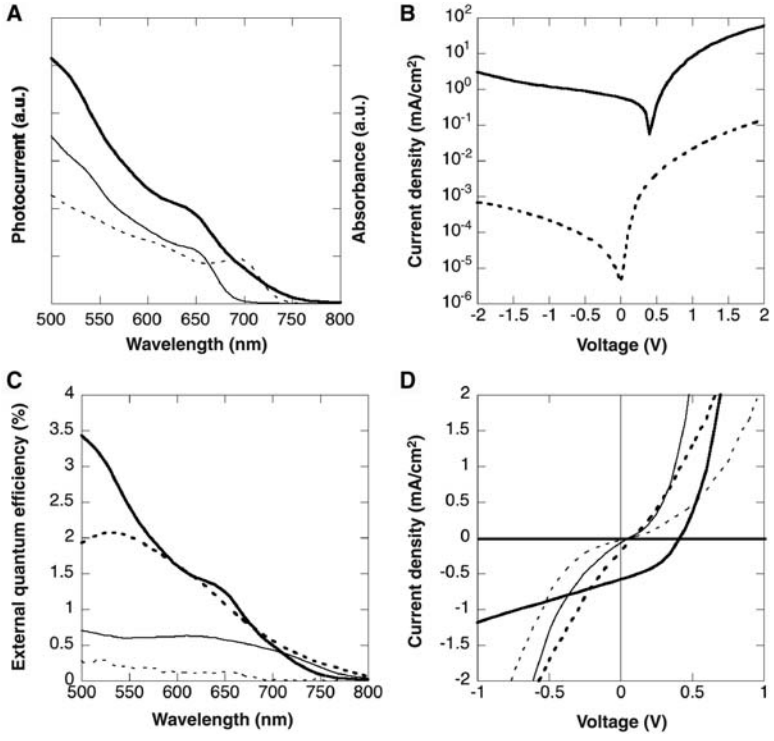

Fig. 2. (**A**) The normalized photocurrent spectral response of a typical ITO/100-nm CdTe/100-nm CdSe/Al bilayer device (bold) is illustrated alongside solution-phase absorption spectra for the CdTe (dotted) and CdSe (solid) NCs from which the device was fabricated. The photoaction spectrum reflects the red CdTe absorption edge and the prominent CdSe exciton peak, indicating that both components are active. a.u., arbitrary units. (**B**) I-V characteristics for this device in the dark (dotted) and under simulated one-sun AM1.5G illumination (solid). The device behaves as a rectifying diode with a notable photovoltaic response. The strong photoconductive response of the device is also illustrated. (**C**) A comparison of external quantum efficiency spectra collected under low-intensity illumination ($\sim 5 \times 10^{-2}$ mW/cm^2). We see significant enhancement in bilayer (bold, solid) and blend (bold, dotted) devices versus a CdTe single-material device (solid) and a CdSe single-material device (dotted), all of comparable optical density. The comparison serves to illustrate the role of charge transfer in photocurrent generation. (**D**) A comparison of I-V characteristics between the set of devices in (C) under simulated AM1.5G illumination. Nearly symmetric I-V behavior in the single-material devices suggests that diode behavior in the bilayer is not simply the result of a Schottky junction with either material. With no contact selectivity, blend cells show negligible rectification and photovoltage.

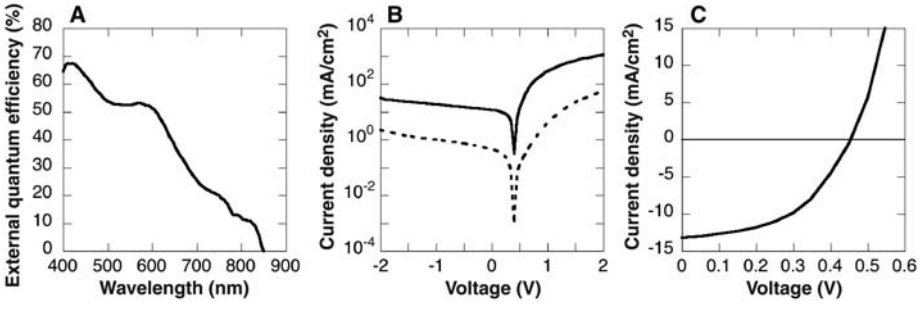

Fig. 3. (**A**) The normalized photoaction spectrum of a typical bilayer device after sintering reveals the broadened spectral response and enhanced quantum efficiency that result from sintering. (**B**) I-V characteristics of a typical bilayer device before sintering (dotted) and after sintering (solid), measured at simulated one-sun AM1.5G illumination. The sintered cell shows over an order of magnitude enhancement in photocurrent whereas the open-circuit voltage remains virtually unchanged. (**C**) The use of a Ca 20-nm/Al 80-nm top contact allows for fabrication of devices with AM1.5G power conversion efficiencies as high as 2.9%.

Accounting for these effectively undoped active materials, we propose a mechanism for PV conversion based on donor-acceptor charge transfer. Those photoexcitations that probe the CdTe/CdSe junction experience an energetic driving force for charge transfer, with holes finding lower energy states in the CdTe and electrons finding lower states in the CdSe. Carrier extraction is driven not by means of a built-in field created from a depletion region of substitutional dopants; rather, extraction is primarily driven by directed diffusion, as dictated by the type II heterojunction (*7*, *9*). After absorption and charge transfer, majority holes in the CdTe readily diffused into the ITO but were blocked from moving through the CdSe toward the Al electrode. Likewise, majority electrons in the CdSe can diffuse only toward the Al, and not through the CdTe to the ITO. The well-accepted metal-insulator-metal model, in which electrodes of disparate work functions equilibrate to form a field across the dielectric active materials, likely provides an additional driving force for carrier extraction.

In order to assess the role of charge transfer in facilitating PV energy conversion, devices composed of a thin film of only one NC material were juxtaposed with cells containing charge transfer junctions between the two types of crystals. All devices had comparable thicknesses of active materials on the order of 200 nm and comparable optical densities across the spectrum. A direct comparison of external quantum efficiencies in the CdTe-only, CdSe-only, and bilayer CdTe/CdSe devices (Fig. 2C) shows a significant enhancement in creation and extraction of carriers due solely to the presence of a charge transfer interface within the device. As is the case in organic systems, separation of electrons and holes across the interface enhances the diffusional driving force for charge extraction while reducing the likelihood of exciton recombination. Devices composed of intimately mixed blends of CdSe and CdTe nanocrystals similarly exhibit enhanced quantum efficiencies over single-material cells (Fig. 2C), offering further evidence that the photoaction of these devices is based on a D-A junction rather than a conventional planar p-n junction.

We also compared the I-V characteristics of these various devices under simulated AM1.5G illumination. As noted above, cells based on heterojunction bilayers exhibit good diode behavior with strong rectification. By comparison, I-V characterization of devices composed of only CdTe or only CdSe showed no

significant rectification (Fig. 2D) (*24*). We can thus deduce that the observed PV effect in the bilayer is not a result of Schottky contacts to either material but rather is due to the intended heterojunction.

Having ruled out the presence of conventional p-n or Schottky junctions, it appears that the bilayer NC cell operates by means of the diffusion-assisted D-A heterojunction typical of organic devices. However, several characteristics of the NC solar cell set it apart from its organic-based counter parts. The most efficient organic solar cells are based on distributed heterojunctions, but devices based on simple blends of donor and acceptor NCs (Fig. 2D) neither rectify nor produce a significant photovoltage. In contrast to organic systems, common electrodes do not readily form selective contacts to either the donor or acceptor NCs. Electrons and holes can be injected into either material, such that blend cells pass current in both forward and reverse bias. Incorporation of blocking layers in future cell designs may allow for further investigation of the blend system.

Another fundamental distinction of the NC system has direct consequences on the performance of these devices. Although a heterojunction is nearly always required to efficiently produce free charges from excitons in organic systems, this is not the case for the NCs used in this study. Rod-shaped nanocrystals with high aspect ratios exhibit little confinement along the length of the rod (*25*). Excitons can thus dissociate over this dimension, creating free carriers throughout the NC film. In organic systems, free carriers are created only when otherwise tightly bound excitons are separated across the D-A junction.

With both free electrons and holes residing in the donor and acceptor materials, carriers are more susceptible to recombination in the NC system. This recombination is compounded by the large presence of surface states on the NCs, which act to trap carriers as they move through the film. Indeed, detrimental recombination losses are apparent in the low quantum efficiency of the NC cell compared with similar devices made from organic semiconductors.

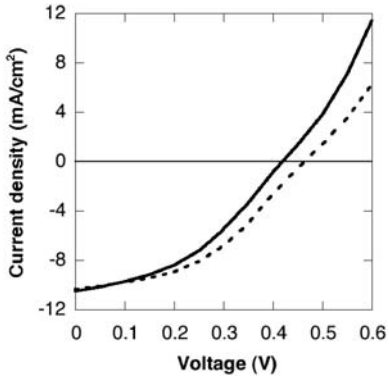

Fig. 4. I-V behavior at simulated one-sun AM1.5G illumination for a typical sintered bilayer device upon first exposure to air (solid) and after 13,000 hours of exposure to ambient atmosphere and light at open circuit. Idle exposure to air and ambient light results in minimal degradation of photocurrent and ultimately affords a 13.6% improvement in overall power conversion efficiency.

We can minimize the high surface trap area inherent in a densely packed array of NCs and concurrently improve carrier transport in the device by annealing and sintering the crystals. Following a well-known technique to facilitate sintering of CdTe thin films (*26*), we exposed NC films to a saturated solution of $CdCl_2$ in methanol and annealed them at 400°C in air for 15 min. After sintering, films of CdSe and CdTe remain insulating in the dark but show about two orders of magnitude enhancement in photoconductivity. The sintering process markedly improves carrier transport but does not appear to result in significant doping.

The photoresponse of sintered CdTe/CdSe bilayer cells mirrors the drastic rise in photoconductivity exhibited by the active layers. A typical photoaction spectrum (Fig. 3A) shows external quantum efficiencies approaching 70% (*27*). As expected, the spectrum reflects a strong red-shift in the onset of photocurrent to the bulk absorption edge. With I_{sc} of 11.6 mA/cm^2, V_{oc} of 0.40 V, and *FF* of 0.45, the resulting solar cell demonstrates a power conversion efficiency of 2.1% under simulated AM1.5G illumination (*28*). The enhancement in efficiency arises solely from the marked increase in photoresponse, whereas cells exhibited a nearly unchanged open-circuit voltage after sintering (Fig. 3B). This result is strong evidence that the driving force for charge extraction is the same in sintered and unsintered devices.

By varying simple system parameters such as electrode material, even higher efficiencies have already been achieved in sintered nanocrystal cells. Figure 3C shows I-V characteristics for the best device fabricated to date, which employs a Ca top contact capped with Al. This cell has an AM1.5G power conversion efficiency of 2.9%, with I_{sc} of 13.2 mA/cm^2, V_{oc} of 0.45 V, and *FF* of 0.49.

None of the solar cells presented here, whether sintered or not, exhibited the strong sensitivity to photo-oxidation characteristic of organic-based devices; in fact, aging seems to improve rather than deteriorate their performance. Figure 4 shows the AM1.5G full-sun behavior of a typical sintered device characterized in air before and after 13,000 hours' open-circuit exposure to ambient atmosphere and lighting. The cell shows only a 1.4% decrease in short-circuit current, whereas the fill factor rose 4.4% and the open-circuit voltage increased by more than 10%. Overall, the atmospheric aging resulted in a 13.6% increase in efficiency. Light-soaking experiments revealed less than 2% degradation in photocurrent after 14 hours at short circuit under simulated AM1.5G illumination with no encapsulation. These phenomena serve to illustrate the robustness of this system over its organic counterparts.

This demonstration introduces solar cells based entirely on colloidal semiconductor nanocrystals. They are ultrathin, solution-processed, and stable in ambient environments. Composed of dense nanocrystal films that mirror the basic properties of semiconducting polymers, these cells function as a class of diffusion-assisted, donor-acceptor heterojunctions. Sintering is found to enhance the performance of these devices, allowing for air-stable power conversion efficiencies up to 2.9%. The nanocrystal solar cells presented here offer an exciting research direction and serve as a key development toward achieving stable and low-cost solar energy conversion.

References and Notes

1. S. E. Shaheen, D. S. Ginley, G. E. Jabbour, *MRS Bull.* **30**, 10 (2005).
2. A. P. Alivisatos, *J. Phys. Chem.* **100**, 13226 (1996).
3. C. B. Murray, C. R. Kagan, M. G. Bawendi, *Annu. Rev. Mater. Sci.* **30**, 545 (2000).
4. M. Shim, C. J. Wang, D. J. Norris, P. Guyot-Sionnest, *MRS Bull.* **26**, 1005 (2001).
5. W. U. Huynh, J. J. Dittmer, A. P. Alivisatos, *Science* **295**, 2425 (2002).
6. B. Q. Sun, H. J. Snaith, A. S. Dhoot, S. Westenhoff, N. C. Greenham, *J. Appl. Phys.* **97**, 014914 (2005).
7. B. A. Gregg, M. C. Hanna, *J. Appl. Phys.* **93**, 3605 (2003).
8. A. J. Nozik, *Phys. E* **14**, 115 (2002).
9. J. A. Barker, C. M. Ramsdale, N. C. Greenham, *Phys. Rev. B* **67**, 075205 (2003).
10. J. J. M. Halls *et al.*, *Nature* **376**, 498 (1995).
11. G. Yu, J. Gao, J. C. Hummelen, F. Wudl, A. J. Heeger, *Science* **270**, 1789 (1995).
12. P. Peumans, V. Bulovic, S. R. Forrest, *Appl. Phys. Lett.* **76**, 2650 (2000).
13. S. E. Shaheen *et al.*, *Appl. Phys. Lett.* **78**, 841 (2001).
14. K. M. Coakley, M. D. McGehee, *Appl. Phys. Lett.* **83**, 3380 (2003).
15. S. Kim, B. Fisher, H. J. Eisler, M. Bawendi, *J. Am. Chem. Soc.* **125**, 11466 (2003).
16. D. J. Milliron *et al.*, *Nature* **430**, 190 (2004).
17. D. S. Ginger, N. C. Greenham, *J. Appl. Phys.* **87**, 1361 (2000).
18. N. Y. Morgan *et al.*, *Phys. Rev. B* **66**, 075339 (2002).
19. J. Heitmann *et al.*, *Phys. Rev. B* **69**, 195309 (2004).
20. Materials and methods are available as supporting material on *Science* Online.
21. Results presented are based on devices that use the standardized syntheses of CdTe and CdSe described above. Other syntheses have yielded slightly different results. For instance, devices with open-circuit voltages as high as 0.6 have been achieved by varying NC diameter; a thorough description of this dependence will be described elsewhere.
22. S. M. Sze, *Physics of Semiconductor Devices* (Wiley, New York, 1981).
23. A. L. Fahrenbruch, R. H. Bube, *Fundamentals of Solar Cells* (Academic Press, New York, 1983).
24. Devices composed of intimately mixed blends of CdSe and CdTe NCs show lower short-circuit currents than bilayer devices, despite comparable external quantum efficiencies (Fig. 2C). This can be attributed to the difference in illumination conditions between these two measurements. Because of instrument limitations, spectral response curves were measured at nearly four orders of magnitude lower illumination intensity than the simulated 100-mW/cm^2 AM1.5G conditions used in I-V comparisons. Increased leakage and recombination in the

blend devices are likely responsible for this discrepancy, but further investigation is needed to fully understand this effect.
25. L. S. Li, J. T. Hu, W. D. Yang, A. P. Alivisatos, *Nano Lett.* **1**, 349 (2001).
26. B. E. McCandless, L. V. Moulton, R. W. Birkmire, *Prog. Photovoltaics* **5**, 249 (1997).
27. These ultrathin cells exhibit suboptimal absorptivity, with average optical density of ~0.7. This assumes full back contact reflection such that incident light passes through the film twice.
28. Short-circuit currents obtained under simulated AM1.5G illumination were well matched with those obtained by integrating external quantum efficiency data with the true AM1.5G solar emission spectrum (*20*).
29. We thank A. Radenovic, K. Sivula, U. Bach, D. Milliron, J. Wang, and S. Laubach for research support and valuable discussion. Supported by the Director, Office of Energy Research, Office of Science, Division of Materials Sciences, of the U.S. Department of Energy under contract no. DE-AC02-05CH11231. I.G. further acknowledges the National Science Foundation for support under a Graduate Research Fellowship. Dedicated in loving memory to Benjamin Boussert, Giulia Adesso, and Jason Choy.

Supporting Online Material
www.sciencemag.org/cgi/content/full/310/5747/462/DC1
Materials and Methods

25 July 2005; accepted 20 September 2005
10.1126/science.1117908

Bridging Dimensions: Demultiplexing Ultrahigh-Density Nanowire Circuits

Robert Beckman, Ezekiel Johnston-Halperin, Yi Luo, Jonathan E. Green, James R. Heath*

A demultiplexer is an electronic circuit designed to separate two or more combined signals. We report on a demultiplexer architecture for bridging from the submicrometer dimensions of lithographic patterning to the nanometer-scale dimensions that can be achieved through nanofabrication methods for the selective addressing of ultrahigh-density nanowire circuits. Order $\log_2(N)$ large wires are required to address N nanowires, and the demultiplexer architecture is tolerant of low-precision manufacturing. This concept is experimentally demonstrated on submicrometer wires and on an array of 150 silicon nanowires patterned at nanowire widths of 13 nanometers and a pitch of 34 nanometers.

One of the central challenges of nanotechnology is the selective addressing of and interaction with individual nanostructures at high densities (i.e., densities limited only by the intrinsic size and packing of the nanostructures). Specifically, this challenge manifests over a range of problems, including coupling of conventional electronics to novel nanoelectronic devices (*1*), addressing of single nanoparticles for applications in quantum computing (*2*), and construction of high-density biomolecular sensor (*3*, *4*) circuits. For nanoelectronics, this challenge relates to the ability to address circuits that have characteristic wire dimensions and pitches that are smaller than the resolution achievable through lithographic patterning. Several groups have reported on methods for fabricating ultrahigh-density nanowire arrays (*4*–*9*).

Architectural concepts for meeting the challenge of electrically addressing (demultiplexing) individual nanowires that are patterned at sublithographic densities should satisfy three criteria. First, the demultiplexer architecture must bridge from the micrometer or submicrometer dimensions achievable through lithography to the few-nanometer dimensions achievable through alternative patterning methods. Second, the architecture should allow for the addressing of many nanowires with a few large wires. Third, the manufacture of the demultiplexer should be tolerant of fabrication defects.

Proposed demultiplexer architectures (*10*, *11*) have been based on combining crossbars (*12*) (lithographically patterned demultiplexing address wires crossing the nanowires) with multi-input binary tree demultiplexers (*13*). Binary trees, by their very nature, exhibit order $2[\log_2(N)]$ scaling, where N is the number of nanowires and $2[\log_2(N)]$ is the number of the large demultiplexing wires used to address the nanowires. Nanowire assemblies are often characterized by some randomness in organization, as well as by defects such as broken or nonconducting nanowires. To compensate, the proposed schemes contain a certain amount of redundancy (extra wires). The major cost of this redundancy is that the use of additional address wires implies that certain nanowire addresses will be redundant or nonactive; circuit testing must then be carried out to determine the good addresses, and memory must be devoted to storing those addresses (*14*). Kuekes and Williams (*10*) described a diode- or resistor-based decoder that uses $5[\log_2(N)]$ large microscale address wires crossing an array of N nanowires. DeHon *et al.* (*11*) described an architecture that uses no more than $2.2[\log_2(N)] + 11$ address wires. Their scheme is based on the field-effect gating of nanowires by the demultiplexer, and it requires control over the doping profile along the axial dimension of the nanowires. Such nanowires have been realized experimentally (*15*–*17*), and Lieber's group has used them to demonstrate a demultiplexer that bridges fabrication methods (i.e., self-assembly versus lithographic patterning) but not length scales (*18*). Both schemes are based on placing controllable regions on the surface of the nanowires. An individual nanowire, which is initially in the nonconducting state, will conduct only when all of the control regions are field- or voltage-addressed; that is, it is the logical equivalent of a multi-input AND gate.

Here, we describe an electric field effect–based demultiplexing scheme that is tolerant of manufacturing defects, is not seriously limited in terms of the wire size and pitch of the demultiplexer structure, and uses $2[\log_2(N)] + R$ microwires to address N nanowires, where R (for redundant address lines) is zero or a small integer (*14*). This scheme does not require control over the axial doping profile of the underlying nanowires but can take advantage of readily achieved vertical doping profiles, and it is designed to bridge length scales. It is optimized (i.e., R is small) for nanowires for which the pitch and width of the nanowire array are precisely controlled. The scheme is based on NOR logic; that is, the only nanowire that is not field-addressed is the one selected. We first illustrate the feasibility of this concept by demultiplexing an array of Si wires 200 nm wide, patterned at a pitch of 1 μm. We then extend this approach to demultiplexing an array of 150 nanowires at a pitch of 34 nm with individual wire widths of 13 nm. Finally, we identify specific materials development pathways that should allow the full and robust realization of this architecture.

The multiplexer concept is shown in Fig. 1. Here, 2^5 (= 32) nanowires are addressed with five pairs of (drawn) large wires. Note that the binary tree pattern extends above and below the nanowire array. This eases the vertical alignment requirements: As long as the multiplexer pattern is oriented perpendicular to the nanowire array and the nanowire pitch and width dimensions are well defined, the circuit will function (*14*). This aspect of the architecture makes it particularly amenable to patterning methods such as nanoimprint molding (*19*, *20*). The major cost associated with giving up vertical alignment precision is the knowledge of exactly which nanowire is selected by a given input address. For example, the binary address "1 0 1 0 1" used in Fig. 1 corresponds

Division of Chemistry and Chemical Engineering, California Institute of Technology, MC 127-72, 1200 East California Boulevard, Pasadena, CA 91125, USA.

*To whom correspondence should be addressed. E-mail: heath@caltech.edu

ERRATUM

post date 9 December 2005

Reports: "Air-stable all-inorganic nanocrystal solar cells processed from solution" by I. Gur *et al.* (21 Oct. 2005, p. 462). On page 464, in two places, it is mentioned that an aging experiment was carried out for 13,000 hours. These instances should read ~13,000 minutes. These errors occur in line 4 of the Fig. 4 caption and in column 2, fourth paragraph, line 8.